Physiological and Molecular Plant Pathology 143 (2026) 103111

Contents lists available at ScienceDirect

Physiological and Molecular Plant Pathology

journal homepage: www.elsevier.com/locate/pmpp

Metabarcoding reveals rhizosphere microbiome differences in healthy and basal rot-affected dragon fruit plants

Marly Guelac Santillan [a,b], Paul Fernandez Castro [d], Angel F. Huaman Pilco [a,b], Richard Estrada [e], Pedro Rodríguez Grados [a,b], Carlos I. Arbizu [a,b,c,*]

[a] Grupo de Investigación en Patología Intracelular de Plantas, Instituto de Investigación para el Desarrollo Sustentable de Ceja de Selva, Universidad Nacional Toribio Rodríguez de Mendoza de Amazonas (UNTRM), Chachapoyas, 01001, Amazonas, Peru
[b] Grupo de Investigación en Raíces y Tuberosas (GIRT), Centro de Investigación en Germoplasma Vegetal y Mejoramiento Genético de Plantas (CIGEMP), Universidad Nacional Toribio Rodríguez de Mendoza de Amazonas, Chachapoyas, 01001, Amazonas, Peru
[c] Facultad de Ingeniería y Ciencias Agrarias, Universidad Nacional Toribio Rodríguez de Mendoza de Amazonas, Chachapoyas, Amazonas, 01001, Peru
[d] Instituto de Investigación en Ganadería y Biotecnología (IGBI), Universidad Nacional Toribio Rodríguez de Mendoza de Amazonas, Chachapoyas, Amazonas, 01001, Peru
[e] Dirección de Desarrollo Tecnológico Agrario, Instituto Nacional de Innovación Agraria (INIA), Lima, Peru

ARTICLE INFO

Keywords:
Basal rot
Metabarcoding
Microbiome dysbiosis
Rhizosphere
Soil diversity

ABSTRACT

The rhizosphere microbiome plays a crucial role in plant health, yet its dynamics in *Selenicereus megalanthus* (yellow dragon fruit) remain poorly understood. This study employed high-throughput sequencing to characterize the bacterial and fungal communities in the rhizosphere of healthy and basal rot-affected plants across four commercial production sites in Amazonas department from Peru. Amplicon sequencing Metagenomics Sequencing (WOBI) targeting to 16S rRNA (for bacteria) and ITS (for fungi) gene regions show differences in microbial community structure associated with plant health status. Multivariate analyses revealed a clear disease-driven reassembly of the bacterial microbiome, marked by the loss of health-associated taxa (*Xanthobacteraceae*, *Geminicoccaceae*, *Nocardioidaceae*) and enrichment of oligotrophic and stress-tolerant groups (*Nitrososphaeraceae*, *Acidobacteriaceae* Subgroup 1). In contrast, fungal assemblages displayed structural inertia, responding primarily through pathogen-associated increases in *Nectriaceae*. Soil physicochemistry articularly pH, exchangeable aluminum, and nutrient levels modulated the strength of bacterial differentiation, highlighting the role of edaphic filters in microbiome resilience.

Our findings provide evidence of a bacterial-centered dysbiosis associated with basal stem rot in *S. megalanthus*, while positioning fungal communities as structurally resilient components of the holobiont. Together, these results outline a framework in which disease is linked to altered plant microbe soil feedbacks rather than pathogen presence alone, and suggest that bacterial assemblages could inform the development of microbiome-based early-warning indicators and soil health strategies for sustainable dragon fruit management.

1. Introduction

Yellow dragon fruit (*Selenicereus megalanthus*), a member of the Cactaceae family, is native fruit to the tropical regions of South America, particularly distributed in Ecuador, Colombia, Peru, and Bolivia [1]. Its cultivation has expanded into tropical and subtropical regions due to its drought tolerance and adaptability, making it a promising crop for arid environments. In addition, its nutritional value and antioxidant content, this fruit has gained significant attention in international markets [2,3]. The fruit is highly appreciated for its nutritional and medicinal properties [4]. and has gained significant attention in domestic and international markets due to its high content of vitamins, antioxidants, fiber, and essential minerals [5]. However, this expansion has been accompanied by increasing phytosanitary challenges, including fungal diseases that significantly impact crop productivity [6].

Although *S. megalanthus* is widely cultivated across South America, it is highly susceptible to phytopathogens, posing serious threats to production and sustainability [7]. In this context, soil microorganisms play

* Corresponding author. Grupo de Investigación en Patología Intracelular de Plantas, Instituto de Investigación para el Desarrollo Sustentable de Ceja de Selva, Universidad Nacional Toribio Rodríguez de Mendoza de Amazonas (UNTRM), Chachapoyas, 01001, Amazonas, Peru.
E-mail address: carlos.arbizu@untrm.edu.pe (C.I. Arbizu).

https://doi.org/10.1016/j.pmpp.2026.103111
Received 10 June 2025; Received in revised form 2 January 2026; Accepted 3 January 2026
Available online 6 February 2026

a critical role in terrestrial ecosystems, contributing to productivity, community composition, plant health [8], and mediating ecosystem responses to environmental factors [9]. The plant soil interface, known as the rhizosphere, is a microbial diversity hotspot, harboring communities distinct from bulk soil [10]. and this has driven a shift from individual microbial studies to a community-level perspective [11]. Despite substantial advances in soil microbiome research, important gaps remain due to the high taxonomic diversity, functional redundancy, and environmental context-dependency of plant–soil–microbe interactions [10,12].

Within the rhizosphere, both beneficial and harmful microorganisms coexist. Beneficial microbial taxa can promote plant growth, enhance nutrient acquisition, or suppress soil-borne pathogens [13,14] whereas harmful microorganisms, particularly phytopathogens, can significantly reduce crop performance [15]. In dragon fruit cultivation, bacterial and fungal pathogens are major contributors to yield losses [16].

Key pathogens such as *Botryosphaeria dothidea*, *Colletotrichum gloeosporioides*, and *Fusarium oxysporum* have been linked to stem and fruit rot, often leading to crop abandonment in severe cases [17]. Basal rot has emerged as one of the most economically damaging diseases, affecting up to 70% of export-grade fruit [18]. Soft stem rot, in particular, compromises fruit quality and yield [7,19]. *F. oxysporum*, a highly aggressive soil-borne pathogen also reported on *Prunus cerasifera* in Spain [20]. has been confirmed as the causal agent of basal rot in pitahaya in Peru, with reported infection rates up to 100% [21].

High-throughput sequencing (HTS) using Amplicon Metagenomics Sequencing has become an essential tool for profiling microbial communities, enabling in-depth analyses of their variability in relation to plant species and health status [22].

We hypothesize that basal rot in *S. megalanthus* results from the interaction of multiple biotic and abiotic factors, which induces quantifiable shifts in the bacterial and fungal communities of the rhizosphere. Specifically, we expect to observe significant differences in the diversity and composition of both bacteria and fungi between healthy and diseased plants. This study is the first to integrate metabarcoding analyses across four geographically distinct sites in the Amazonas department, providing novel insights into how environmental context shapes microbiome responses to basal rot in pitahaya.

2. Materials and methods

2.1. Field description and sampling

A total of 45 samples were collected from four production sites belong to Amazonas department, Peru: Matiaza Rimachi, Cocahuyco, Cochamal, and Huambo, where both healthy and basal rot-affected plants were diagnosed and sampled (Fig. 1) Table 1. Soil samples were collected from four cardinal points around each plant, at a distance of 50 cm from the stem and a depth of (0_ 30 cm), following the protocol of [23]. The top layer of leaf litter was removed using a hand shovel. The four subsamples collected per plant were thoroughly homogenized to obtain a single composite sample, after that, the sample were transported to the Plant Health Laboratory of Universidad Nacional Toribio Rodriguez de Mendoza for physicochemical and molecular studies. Each plant represented one biological replicate, and plants were separated by at least 10–15 m to ensure sample independence. Bulk soil was not included as a control for this study.

2.2. Physicochemical soil analysis

Rhizospheric soil samples were collected by operationally defining this fraction as the soil firmly adhering to the root zone, obtained after gently removing loose bulk soil. Following collection, samples were first preserved at −20 °C and subsequently stored at −80 °C until processing for DNA extraction. Soil physicochemical analyses were conducted at the Soil and Water Research Laboratory (LABISAG) of the Universidad Nacional Toribio Rodríguez de Mendoza de Amazonas (UNTRM). The evaluated parameters included pH (measured using a potentiometer with a 1:1 soil-to-water ratio), electrical conductivity (EC), available phosphorus (modified Olsen method), exchangeable potassium (ammonium acetate extraction, pH-adjusted), soil texture (hydrometer method), and organic matter content (Walkley and Black method). All procedures followed the EPA 3050B protocol and the Mexican official standard NOM-021-RECNAT-2000.

2.3. DNA extraction and amplicon sequencing

Total DNA was extracted from 250 mg of rhizospheric soil using the DNeasy PowerSoil® Kit (QIAGEN, Hilden, Germany), according to the manufacturer's instructions. DNA quality and concentration were

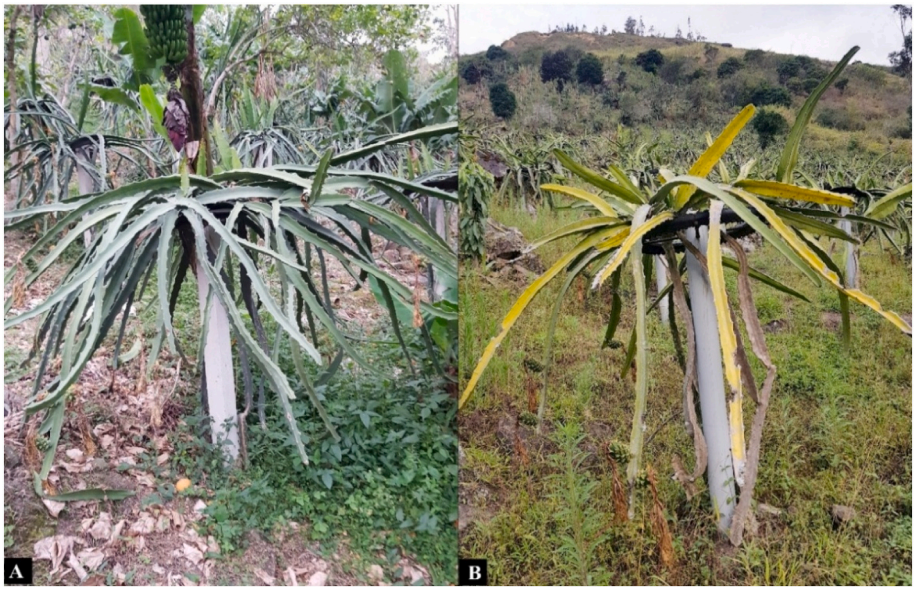

Fig. 1. A. Healthy plants with good color in the stems and roots. B. Diseased plant, showing yellow to brown coloration in the stem and roots. (For interpretation of the references to color in this figure legend, the reader is referred to the Web version of this article.)

Table 1
Cultural practices and crops prior to the planting of yellow pitaya in the different sites sampled.

Parcel	Coordinates	Altitude (m)	Age of orchard	Trellising	Fertilization			Soil type	Irrigation	Previous crops
					N	P	K			
Matiaza Rimachi (Mati)	6°02′29.4″S 77°55′58.9″W	1591	Five	Yes	120	130	150	sandy loam soil	Drip irrigation	Corn, Cassava
Cocahuyco (Cocah)	6°03′26.9″S 77°55′27.0″W	1590	Five	Yes	120	130	150	sandy loam soil	Drip irrigation	Cassava
Cochamal (Coch)	6°24′58.0″S 77°34′46.3″W	1456	Five	Yes	120	130	150	sandy loam soil	Rainfed	Corn, Coffee
Huambo (Huam)	6°25′40.4″S 77°31′01.9″W	1443	Five	Yes	120	130	50	cleym loam soil	Rainfed	Cassava

Note: Previous agricultural characteristics and practices of the plot.

assessed via 0.8% agarose gel electrophoresis stained with GelRed and quantified using a Qubit® 3.0 Fluorometer (Invitrogen, USA). High-quality DNA samples were stored at −20 °C and sent for sequencing to a commercial genomic facility in (Novogene) China, using the Illumina MiSeq platform.

The V3–V4 region of the 16S rRNA gene and the ITS region were amplified using the primer pairs 341F/806R and ITS3-2024F/ITS4-2409R, respectively. Both libraries were sequenced using a paired-end (2 × 150 bp) format, yielding amplicons of approximately 428 bp [24].

2.4. Bioinformatics analysis

Bioinformatic processing was performed using the nf-core/ampliseq pipeline (version 2.15.0; https://doi.org/10.5281/zenodo.17279391) [25], which is part of the nf-core workflow collection [26]. Reproducible software environments were provided through Bioconda [27] and Biocontainers [28]. The workflow was executed with Nextflow v4.2.1 [29] within a Singularity container.

Data quality was assessed using FastQC [30], and summary reports were generated with MultiQC [31]. Sequence processing was carried out with DADA2 [32], A total of 45 samples were sequenced targeting the 16S rRNA and ITS regions, yielding 16,668,612 and 17,535,144 raw reads, respectively. Rarefaction curves based on Abundance-based Coverage Estimator (ACE), Chao1, and observed OTUs showed a stabilization trend (S1 and S2 Fig; Table S1), indicating sufficient sequencing depth. These findings are consistent with those reported by Ref. [20]. The plateau in by the curves confirms adequate coverage microbial diversity captured which included the removal of PhiX contamination, truncation of reads with quality scores ≤2, trimming before the median quality dropped below 25, and retention of at least 75% of the input reads. Demultiplexing, paired-end read merging, PCR chimera removal, and the inference of amplicon sequence variants (ASVs) were also performed using the DADA2 algorithm.

Taxonomic assignment was conducted in DADA2, using a minimum bootstrap confidence threshold of 50 (from 100 iterations). For bacterial sequences, the SILVA 138.2 Prokaryotic SSU database was used as reference [33].

ASVs, their abundances, and taxonomic annotations were imported into QIIME2 [34]. ASVs identified as mitochondria or chloroplast were removed prior to further analyses. Within QIIME2, microbial community composition was visualized using bar plots, and sequencing depth was evaluated with alpha-rarefaction curves.

Functional potential of the bacterial microbiota was predicted using PICRUSt2 [35], which estimated the relative abundance of genes and metabolic pathways. Functional predictions were categorized according to KEGG Orthology (KO), Enzyme Commission (EC), and MetaCyc databases, and visualized through heatmaps and functional enrichment plots.

2.5. Statistical analyses

Diversity, abundance, and rarefaction analyses were conducted using the Bioconductor framework and the Phyloseq package [36]. Additional analyses were implemented through custom scripts using the Microeco [37]. and MicrobiomeMarker packages. The MicrobiotaProcess package [38] was specifically used to generate LDA plots, Venn diagrams, and cladograms.

Alpha diversity metrics including the Shannon index, Pielou's evenness, and the number of observed operational taxonomic units (OTUs) were calculated. Group differences were assessed using the non-parametric Kruskal Wallis test, with Bonferroni correction applied for multiple comparisons.

To assess community structure, dimensionality reduction was performed through Principal Component Analysis (PCA), exploring variation in the relative abundances of major taxa. Beta diversity patterns were evaluated using Principal Coordinates Analysis (PCoA) based on distance or dissimilarity matrices. Statistical significance between groups was tested using PERMANOVA with 999 permutations.

Data visualization was carried out in R version 4.4.1, using the packages RColorBrewer [39], ComplexHeatmap [40], and ggplot2 [41].

3. Result

3.1. Alfa diversity

Bacterial communities in healthy plants exhibited significantly higher diversity, richness, evenness, and phylogenetic diversity compared to diseased plants (S3 Fig; Table S2). In contrast, fungal communities showed no significant differences between conditions, suggesting a relatively stable structure.

Alpha diversity exhibited contrasting patterns between bacterial and fungal communities according to plant health status. For bacteria (Fig. 2A), the Shannon index revealed significantly higher diversity in healthy plants, with marked reductions in diseased rhizospheres from Cocahuayco and Cochamal (p-values ranging from 0.026 to 0.31). These findings indicate a clear decline in bacterial community complexity under disease conditions. Consistently, Faith's phylogenetic diversity (Fig. 2B) was also lower in diseased plants, with statistically significant differences in Huambo ($p = 0.032$) and similar trends in Cocahuayco and Cochamal, suggesting a loss of evolutionary lineages in pathogen-affected soils.

In contrast, fungal communities displayed much greater stability between healthy and diseased plants. Shannon diversity for fungi (Fig. 2C) showed no significant differences across sites ($p > 0.05$), indicating that *Fusarium oxysporum* infection did not substantially alter fungal richness or evenness. Faith's PD for fungi (Fig. 2D) followed the same pattern, with comparable values across health conditions and only minor, non-significant fluctuations. This stability suggests that the fungal component of the rhizosphere microbiome is less sensitive to disease-driven perturbations than bacterial communities. Taken together, these results demonstrate that basal rot primarily disrupts bacterial diversity both taxonomic and phylogenetic while fungal diversity remains relatively unaffected. This supports the notion that bacterial communities are more responsive to biotic stress in the

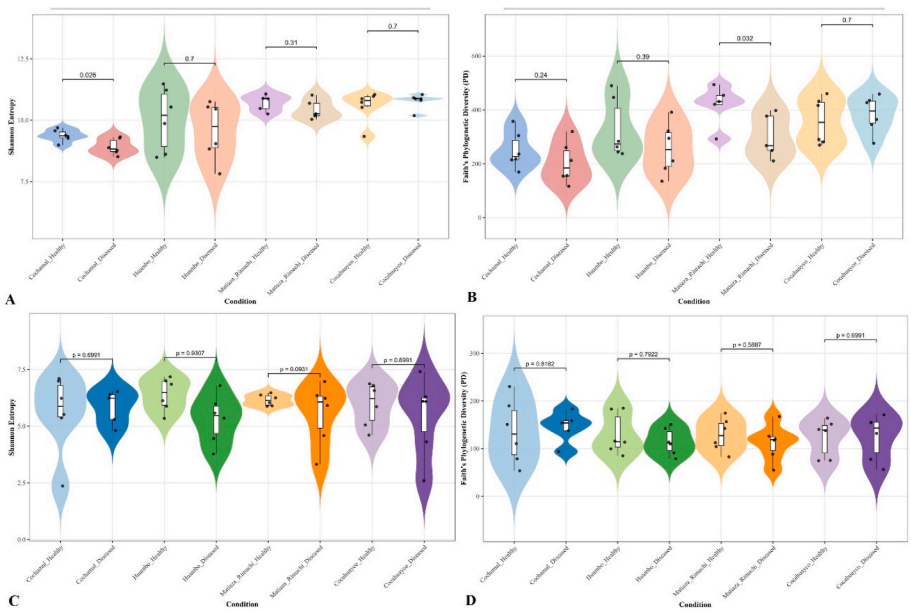

Fig. 2. Alpha diversity of bacterial and fungal communities associated with healthy and basal rot affected *Selenicereus megalanthus* plants. Shannon diversity and Faith's Phylogenetic Diversity (PD) are shown for bacterial 16S communities (A, B) and fungal ITS communities (C, D).

rhizosphere and may serve as more sensitive indicators of disease-associated shifts in soil microbiome structure.

3.2. Beta diversity

3.2.1. Bacterial communities (16S rRNA)

PCA based on family-level relative abundance revealed clear shifts in bacterial community composition between healthy and basal rot-affected plants within each locality (Fig. 3). In Cochamal and Huambo, healthy and diseased rhizospheres formed well-defined and minimally overlapping clusters along PC1, indicating strong disease-associated restructuring of the bacterial microbiome.

In Matiaza Rimachi and Cocahuayco, separation between health statuses was also evident, though with greater dispersion, suggesting a more heterogeneous response among individual plants. The vectors representing the top five contributing families in each locality highlighted distinct taxonomic signatures. Families such as *Xanthobacteraceae, Geminicoccaceae,* and *Nocardioidaceae* tended to align with healthy rhizospheres groups frequently associated with nutrient cycling and plant-beneficial functions whereas families enriched toward diseased samples (*Nitrososphaeraceae, Acidobacteriaceae* Subgroup 1) reflected taxa often favored under stress or dysbiotic conditions. Together, these patterns demonstrate that basal rot induces pronounced and site-specific reorganization of bacterial communities in the rhizosphere of *S. megalanthus*.

3.2.2. Fungal communities (ITS)

In contrast to bacteria, the ITS-based PCA showed weaker and less consistent separation between healthy and diseased plants across the four localities (Fig. 4). Although certain families most notably *Nectriaceae*, which includes *Fusarium oxysporum,* and *Aspergillaceae* displayed directional association with diseased plants in specific sites, the overall clustering patterns exhibited substantial overlap between health statuses.

These results indicate that fungal communities in the rhizosphere are more structurally stable and show limited community-level responsiveness to basal rot compared with bacterial communities. Observed changes appear to be driven by localized increases in specific taxa, rather than broad shifts in fungal community organization.

Additional analyses using Jaccard and unweighted UniFrac metrics revealed both taxonomic and phylogenetic differences related to plant health status in bacterial and fungal communities (Fig. S4A-D and Fig. S5A-B). Notably, fungal communities in Cocah exhibited distinct clustering between healthy and diseased plants, highlighting the strong influence of disease on microbial structure in that location.

3.3. Taxonomic composition of fungal and bacterial communities

The rhizosphere microbial communities displayed marked taxonomic differences between healthy and diseased plants (Fig. 5). Among bacteria, distinct patterns were observed in the relative abundance of key phylum including *Actinobacteriota*, *Proteobacteria*, *Acidobacteriota*, *Chloroflexota*, and *Crenarchaeota*. *Actinobacteriota* was more abundant in soils from diseased plants, whereas, as an *Proteobacteria* dominated in healthy plant soils, suggesting its association with beneficial microbiome functions (Table S3). *Acidobacteriota* was particularly enriched in Cocah, possibly reflecting specific edaphic factors.

At the bacterial order level, *Frankiales* and *Rhizobiales* were more prevalent in diseased soils, while *Vicinamibacterales* and *Gaiellales* were enriched in healthy soils, indicating potential roles as indicators of microbial stability.

For the fungal communities, *Ascomycota* was the dominant phylum, especially in healthy plants from Huam, followed by *Basidiomycota* and *Rozellomycota*, which were more abundant in diseased plants from Coch (Table S4). At the order level, *Hypocreales* and *Eurotiales* were enriched in Huam and Cocah, while *Trechisporales*, *Helotiales*, and *Agaricales* showed specific ecological distributions. These findings suggest that plant disease may favor the proliferation of less dominant and potentially opportunistic fungal taxa, thereby altering the rhizosphere microbiome structure.

3.4. Soil physicochemical parameters on diseased and healthy plants

The results demonstrate that soil physicochemical properties have a direct impact on pitahaya plant health. In the Mati and Cocah sites, neutral pH values favored microbial stability and nutrient availability. In contrast, the highly acidic pH in Coch may compromise plant defense mechanisms. In Huam, a moderately acidic pH combined with elevated potassium levels may enhance plant resistance to pathogens.

Correlation coefficients are displayed using a color scale, where red

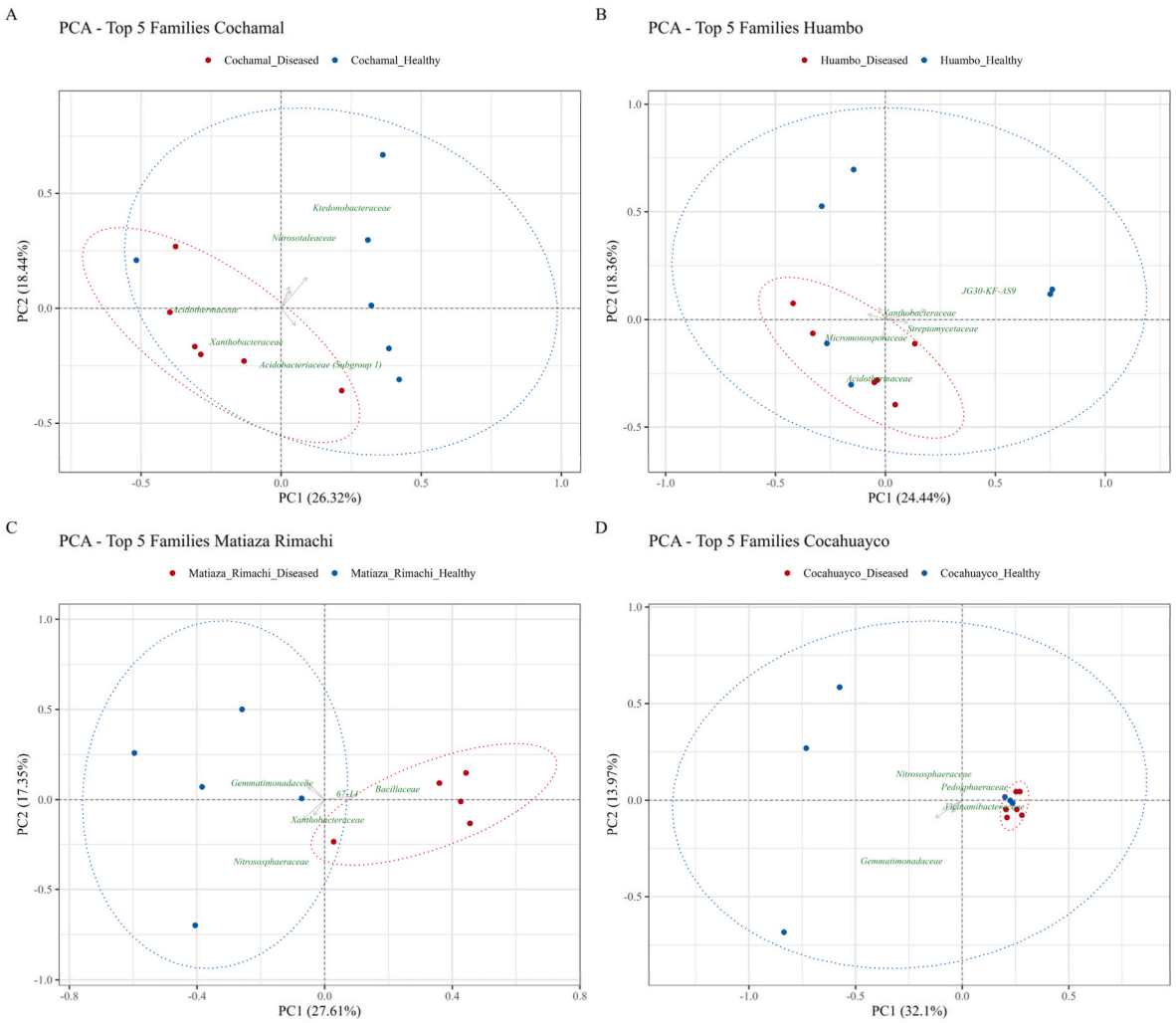

Fig. 3. Principal Component Analysis (PCA) of beta diversity based on the five most abundant bacterial families across four sampling sites. PCA ordination illustrates the compositional differences between healthy and basal rot–affected plants at (A) Cochamal, (B) Huambo, (C) Matiaza Rimachi, and (D) Cocahuayco. The first two principal components (PC1 and PC2) explain a moderate proportion of the total variance and reveal distinct clustering patterns associated with plant health status.

tones indicate positive correlations and yellow tones indicate negative correlations. Abbreviations correspond to soil pH (pH), electrical conductivity (EC), phosphorus (P), potassium (K), calcium (Ca), magnesium (Mg), sodium (Na), organic matter (OM), nitrogen (N), exchangeable aluminum (Al^{3+}), cation exchange capacity (CEC), and soil diversity (S_D), among other analyzed variables.earson's correlation of analysis.

All sampled plots exhibited a clay loam texture, which is optimal for moisture and nutrient retention. Coch had the highest phosphorus content, potentially stimulating phosphate-mineralizing microorganisms. It also exhibited elevated organic matter levels, which may support the proliferation of saprotrophic fungi. While organic carbon content remained relatively stable across sites, nitrogen levels were consistently low, which may limit plant growth. These findings highlight the importance of proper soil management to reduce disease pressure in pitahaya cultivation.

Heat map of, Pearson's correlation displayed. In healthy plants, a strong positive correlation was observed between pH and Calcium Ca^{2+} ($r = 0.94$), while organic carbon showed a negative correlation with base saturation (S_B) (Fig. 6A). While in diseased plants organic matter and carbon were perfectly correlated ($r = 1.0$), whereas pH had a strong negative correlation with exchangeable acidity aluminum ($Al^{3+} + H^{+}$; $r = -1.0$) (Fig. 6B).

4. Discussion

Basal stem rot in *S. megalanthus* exerts a profound and asymmetrical impact on the rhizosphere microbiome, strongly restructuring bacterial communities while leaving fungal assemblages comparatively stable. This pattern aligns with previous findings showing that bacteria respond more rapidly and sensitively than fungi to pathogen invasion, root decay, and disruption of rhizodeposition [13,14].

Alpha diversity analyses demonstrated a consistent reduction in bacterial richness, evenness, and phylogenetic diversity in diseased plants across all localities. Healthy rhizospheres showed significantly higher Shannon diversity, a trend frequently observed in wilt-affected crops, where pathogen activity limits carbon availability and suppresses beneficial bacterial groups [15]. The marked decline in Faith's phylogenetic diversity further indicates a loss of entire evolutionary lineages, reducing functional redundancy essential for nutrient turnover, nitrogen transformations, and pathogen antagonism [13]. These patterns represent the classical hallmarks of microbiome destabilization under pathogen pressure and are ecologically meaningful, as reduced bacterial diversity weakens the rhizosphere's capacity to buffer environmental and biotic stress, thereby reinforcing disease progression [42,43].

Beta diversity patterns supported this interpretation. Healthy and diseased bacterial communities formed distinct, minimally overlapping

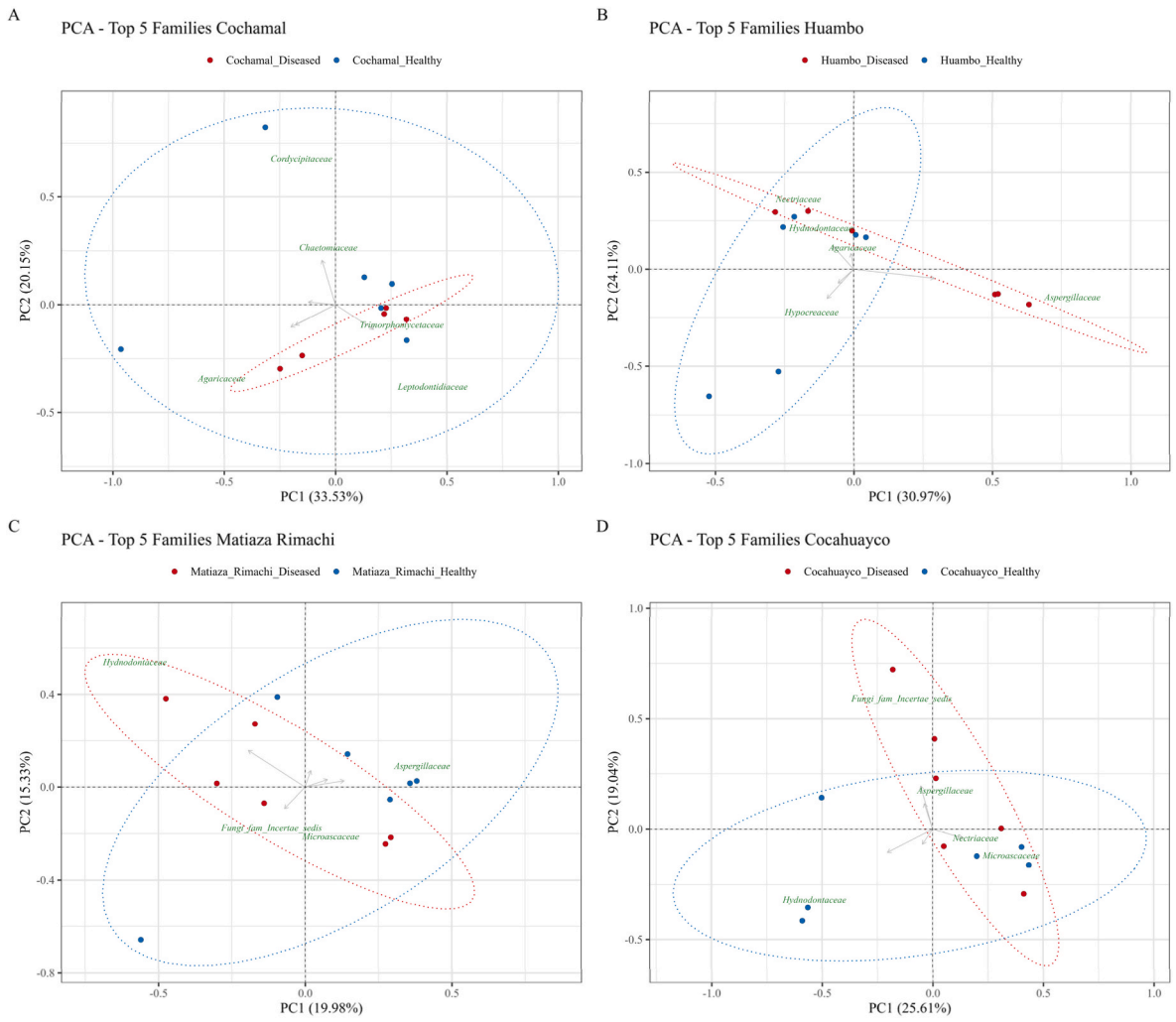

Fig. 4. Principal Component Analysis (PCA) of beta diversity based on the five most abundant bacterial families across four sampling sites. The PCA ordination shows clear differentiation between healthy and basal rot–affected samples at (A) Cochamal, (B) Huambo, (C) Matiaza Rimachi, and (D) Cocahuayco. Although the first two principal components (PC1 and PC2) explain a moderate proportion of the total variance, they reveal distinct clustering patterns associated with plant health status.

clusters particularly in Cochamal and Huambo indicating strong disease-associated restructuring [24,44]. Similar community separation has been documented in plant systems where pathogens alter oxygen gradients, disrupt root exudates, and modify nutrient microhabitats, prompting rapid bacterial turnover [13,14].

Taxonomic shifts revealed mechanistic processes underlying this dysbiosis. Diseased rhizospheres were enriched in Actinobacteriota especially Acidothermaceae groups capable of degrading complex polymers and thriving under acidic, low-carbon, or otherwise stressed conditions [23,45]. Their proliferation likely reflects the combined influence of decreased carbon inputs, tissue necrosis, and altered redox conditions created by *Fusarium oxysporum* infection [20,21].

Conversely, healthy plants were associated with families such as *Xanthobacteraceae, Geminicoccaceae*, and *Nocardioidaceae*, taxa known for nitrogen fixation, carbon cycling, and potential plant-beneficial interactions [23]. These groups play key roles in stabilizing rhizosphere processes and suppressing pathogens through competition, hormonal modulation, and xenobiotic degradation [13,14].

In contrast to bacteria, fungal alpha diversity showed minimal differences between healthy and diseased plants, and β-diversity revealed broad overlap, except for localized separation in Huambo [2,46]. This structural resilience is consistent with the view that fungal communities possess high functional redundancy and are often buffered by persistent hyphal networks, making them less sensitive to short-term disturbances in root exudation [10,14].

Although diseased soils showed increased abundance of Nectriaceae including *F. oxysporum*, the causal agent of basal rot and Aspergillaceae, these changes represent targeted pathogen-driven enrichments rather than broad fungal community restructuring. Similar patterns of pathogen proliferation accompanied by stable overall fungal structure have been observed in perennial crops such as coffee and rice [46,47].

Variation among localities underscores the modulating role of soil properties. Sites with more acidic soils, elevated exchangeable aluminum, or lower nutrient availability (Cochamal) exhibited stronger bacterial shifts, suggesting that edaphic constraints reduce microbial buffering capacity and amplify disease impacts. Soil acidity is well known to suppress beneficial bacteria, promote stress-adapted taxa, and create conditions conducive to pathogen dominance [15,48]. The strong negative correlation between pH and exchangeable Al^{3+} in diseased soils supports the mechanism of aluminum-mediated microbial inhibition, which can weaken plant defenses and hinder microbiome resilience.

Nutrient availability also played a role: neutral pH in Matiaza Rimachi likely supported microbial stability, high potassium in Huambo may enhance plant stress tolerance, and elevated phosphorus in Cochamal can stimulate microbial activity [37,49]. These findings reinforce the concept of soil-mediated susceptibility, where physicochemical factors shape both microbial resilience and plant vulnerability

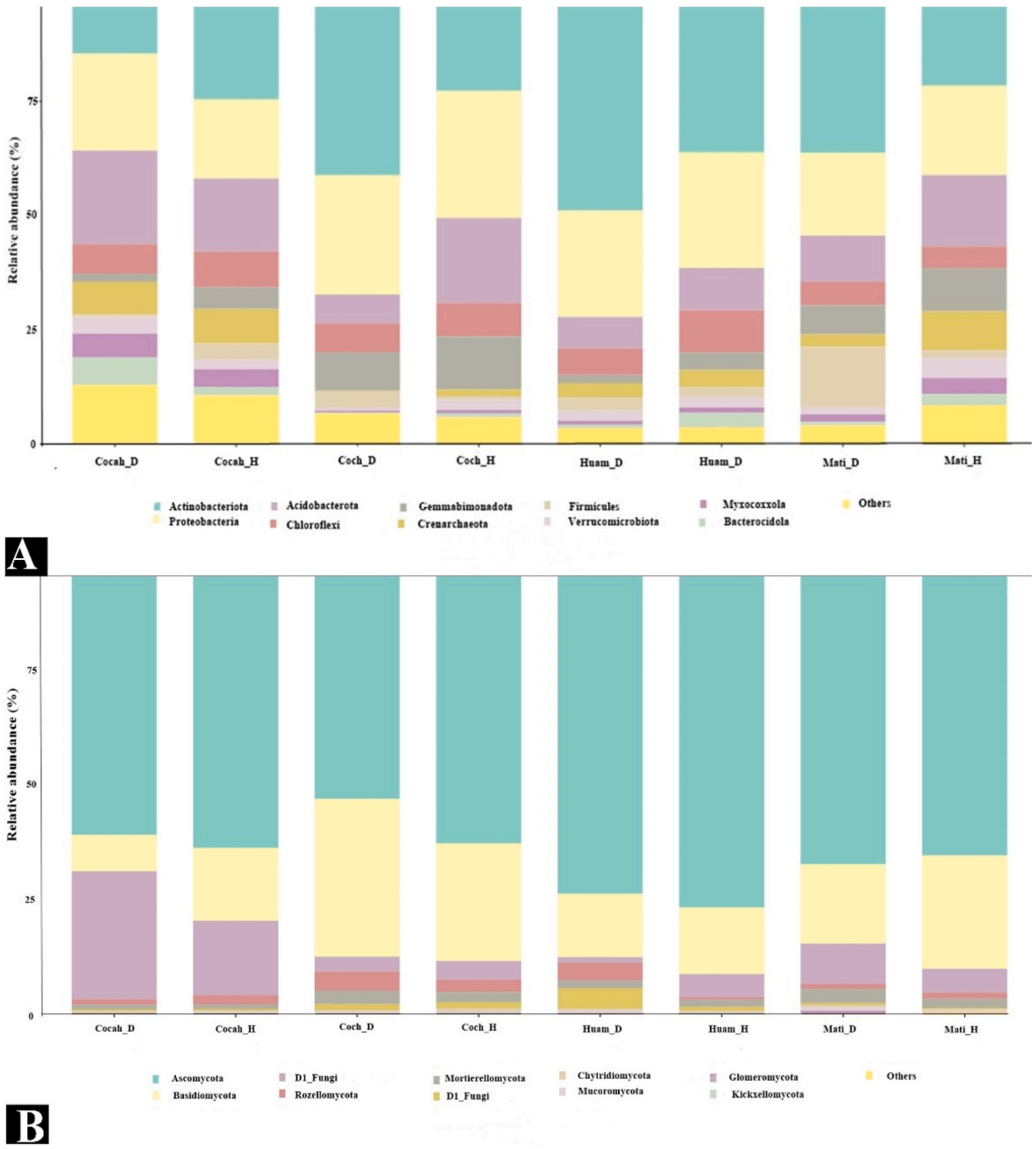

Fig. 5. Relative abundance of dominant microbial phyla in the rhizosphere soil associated with *Selenicereus megalanthus*. (A) Bacterial and archaeal community composition and (B) fungal community composition in healthy (H) and basal rot–affected (D) plants across the different sampling sites.

to disease [13].

Together, the results support a clear mechanistic model in which basal rot induces a bacterial-centered dysbiosis characterized by: Loss of beneficial bacterial groups involved in nutrient cycling, competition, and pathogen suppression, Expansion of oligotrophic and stress-tolerant taxa favored by disease-altered microenvironments. Stable fungal architecture, with pathogen enrichment but no community-wide collapse. Soil physicochemical factors that intensify or mitigate microbiome disruption.

This work provides the first integrative microbial analysis of basal stem rot in *S. megalanthus* and establishes foundational mechanisms linking pathogen activity, soil conditions, and microbiome dysbiosis in pitahaya. By identifying microbial signatures associated with disease and clarifying the ecological processes that drive them, this study offers a framework for developing microbiome-based diagnostics, improving soil management strategies, and guiding the design of microbial inoculants aimed at restoring rhizosphere resilience and enhancing crop sustainability.

5. Conclusion

Basal stem rot in *S. megalanthus* induces a pronounced bacterial dysbiosis, reducing diversity and enriching stress-tolerant taxa, while fungal communities remain structurally stable. These shifts reflect pathogen-driven alterations in root exudation and soil microhabitats. Soil properties, particularly pH and exchangeable aluminum, modulate the severity of microbiome disruption. The identified microbial signatures highlight bacteria as sensitive indicators of plant health. This work provides the first mechanistic framework for microbiome-based monitoring and management of basal rot in yellow dragon fruit.

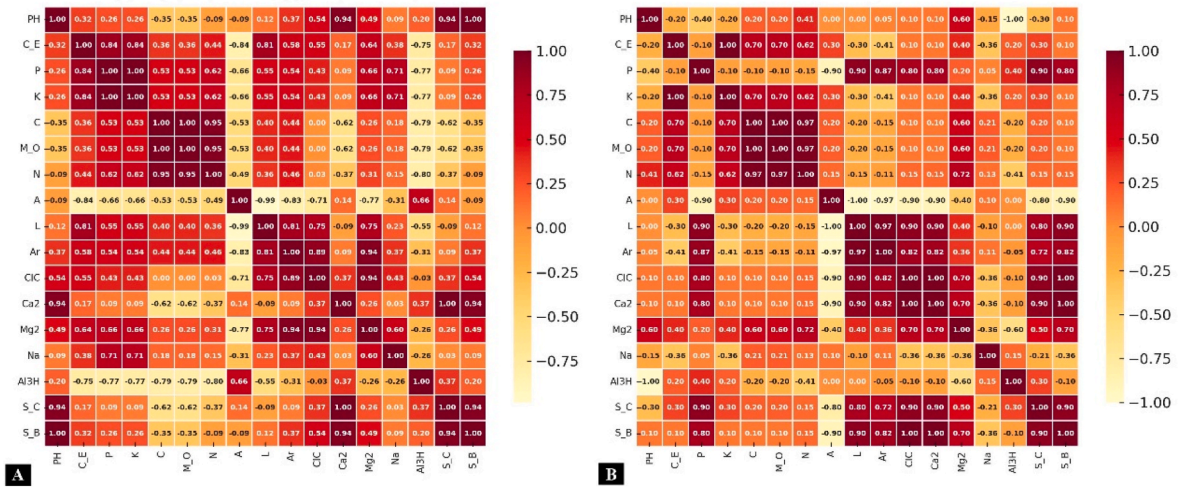

Fig. 6. Pearson correlation analysis among soil physicochemical variables and microbial indices in the rhizosphere (A) Healthy plants and (B) basal rot–affected plants.

CRediT authorship contribution statement

Marly Guelac Santillan: Writing – review & editing, Writing – original draft, Supervision, Software, Resources, Project administration, Methodology, Investigation, Funding acquisition, Formal analysis, Data curation, Conceptualization. **Paul Fernandez Castro:** Writing – review & editing, Writing – original draft, Software, Methodology, Investigation, Formal analysis, Data curation. **Angel F. Huaman Pilco:** Writing – review & editing, Writing – original draft, Supervision, Resources, Project administration, Methodology, Investigation, Funding acquisition, Conceptualization. **Richard Estrada:** Visualization, Data curation. **Pedro Rodríguez Grados:** Resources, Methodology, Investigation. **Carlos I. Arbizu:** Writing – review & editing, Validation, Supervision, Resources, Project administration, Methodology, Investigation, Funding acquisition, Conceptualization.

Funding

This work has been financed by Project No. 2590699: Mejoramiento del Servicio de Promoción de la Ciencia, Tecnología e Innovación Tecnológica en el Centro de Investigación Frutícola "CIF" de la UNTRM - Distrito de Magdalena de la Provincia de Chachapoyas en el Departamento de Amazonas.

Declaration of competing interest

The authors declare that they have no known competing financial interests or personal relationships that could have appeared to influence the work reported in this paper.

Acknowledgments

We are very grateful to the farmers for the permission to their plots for the collection of soil samples, to the administrator for the logistics and Jherson Rojas Vargas for supporting the data collection in the pitahaya field. The authors also thank the UNTRM-Data Science server for facilitating access for data analysis. The Vice Chancellor's Office of Research at Universidad Nacional Toribio Rodriguez de Mendoza de Amazonas provided financial support for article processing charges (APC)

Appendix A. Supplementary data

Supplementary data to this article can be found online at https://doi.org/10.1016/j.pmpp.2026.103111.

Data availability

The raw data supporting the conclusions of this article will be made available by the authors, without undue reservation.

References

[1] S. Harshitha, Y.V. Nikhil Gowda, Abhijith V. Tom, S.P. Likhith Kumar, K.S. Mohan Kumar, A comprehensive analysis of nutritional profile, cultivation techniques, and therapeutic potential of dragon fruit (hylocereus spp.), J. Pharma Insights Res. 2 (2024), https://doi.org/10.69613/9c4q6n55, 075–094.

[2] C. Oliveira, E. Shakiba, D. North, M. McGraw, E. Ballard, M. Barrett-D'amico, G. Glazko, Y. Rahmatallah, Gene-based metagenomic analysis of rhizosphere soil bacteria in arkansas rice crop fields, Agronomy. 12 (2022), https://doi.org/10.3390/agronomy12010222.

[3] D. Prisa, Pitahaya a new superfood: cultivation methods and medicinal properties of the fruit, Indian J. Natural Sci. 12 (2022) 976–997. https://www.researchgate.net/publication/358502994.

[4] H.E. Khoo, X. He, Y. Tang, Z. Li, C. Li, Y. Zeng, J. Tang, J. Sun, Betacyanins and anthocyanins in pulp and peel of red pitaya (Hylocereus polyrhizus cv. Jindu), inhibition of oxidative stress, lipid reducing, and cytotoxic effects, Front. Nutr. 9 (2022), https://doi.org/10.3389/fnut.2022.894438.

[5] T.G. Huy, T.T. Men, N.P.A. Thi, D.T. Khang, Identification of dragon fruit (selenicereus) species in mekong delta based on dna barcode sequences, Biodiversitas. 22 (2021) 4216–4222, https://doi.org/10.13057/biodiv/d221012.

[6] A.R. Trindade, P. Paiva, V. Lacerda, N. Marques, L. Neto, A. Duarte, Pitaya as a new alternative crop for iberian peninsula: biology and edaphoclimatic requirements, Plants. 12 (2023), https://doi.org/10.3390/plants12183212.

[7] J. Soto, C. Cadenas, L. Mattos, C. Trigoso, First report of Enterobacter cloacae as a causative agent of soft rot disease in dragon fruit (Hylocereus undatus) stems in Peru, Peruvian J. Agronomy. 3 (2019) 144, https://doi.org/10.21704/pja.v3i3.1367.

[8] D. Francioli, G. Lentendu, S. Lewin, S. Kolb, DNA metabarcoding for the characterization of terrestrial microbiota—pitfalls and solutions, Microorganisms. 9 (2021) 1–29, https://doi.org/10.3390/microorganisms9020361.

[9] A.C. Melcher, S. Weber, K. Birkhofer, D. Harms, H. Krehenwinkel, To pool or not to pool: pooled metabarcoding does not affect estimates of prey diversity in spider gut content analysis, Ecol. Entomol. (2024), https://doi.org/10.1111/een.13382.

[10] R.R. Molefe, A.E. Amoo, O.O. Babalola, Metagenomic insights into the bacterial community structure and functional potentials in the rhizosphere soil of maize plants, J. Plant Interact. 16 (2021) 258–269, https://doi.org/10.1080/17429145.2021.1936228.

[11] E.B. Aliche, W. Talsma, T. Munnik, H.J. Bouwmeester, Characterization of maize root microbiome in two different soils by minimizing plant DNA contamination in metabarcoding analysis. https://doi.org/10.1007/s00374-021-01555-3/Published, 2021.

[12] J.F. Cobo, R. Baroncelli, G. Le Floch, A. Picot, A novel metabarcoding approach to investigate Fusarium species composition in soil and plant samples, FEMS Microbiol. Ecol. 95 (2019), https://doi.org/10.1093/femsec/fiz084.
[13] R. Mendes, P. Garbeva, J.M. Raaijmakers, The rhizosphere microbiome: significance of plant beneficial, plant pathogenic, and human pathogenic microorganisms, FEMS Microbiol. Rev. 37 (2013) 634–663, https://doi.org/10.1111/1574-6976.12028.
[14] G. Berg, M. Grube, M. Schloter, K. Smalla, Unraveling the plant microbiome: looking back and future perspectives, Front. Microbiol. 5 (2014), https://doi.org/10.3389/fmicb.2014.00148.
[15] A.E. Fadiji, O.O. Babalola, Elucidating mechanisms of endophytes used in plant protection and other bioactivities with multifunctional prospects, Front. Bioeng. Biotechnol. 8 (2020), https://doi.org/10.3389/fbioe.2020.00467.
[16] D. Alem, T. Dejene, J. Geml, J.A. Oria-de-Rueda, P. Martín-Pinto, Metabarcoding analysis of the soil fungal community to aid the conservation of underexplored church forests in Ethiopia, Sci. Rep. 12 (2022), https://doi.org/10.1038/s41598-022-08828-3.
[17] Y. Ortiz, J. Carrillo, Pitahaya (Hylocereus spp.): a short review, Comunicata Scientice 3 (2012) 220–237. www.ufpi.br/comunicata.
[18] C. Salazar, L. Serna, E. Gómez, Caracterización molecular de Fusarium asociado a pudrición basal del fruto en pitahaya (Selenicereus megalanthus), Agron. Mesoam. 27 (2016) 277, https://doi.org/10.15517/am.v27i2.21269.
[19] L.M. Lizarazo, J.E. Másmela, First report of bacteria associated with soft rot in yellow pitahaya (Selenicereus megalanthus haw.) in Colombia crops, Rev. Fac. Nac. Agron. Medellin 77 (2024) 10797–10809, https://doi.org/10.15446/rfnam.v77n3.111234.
[20] J. Ordóñez, A.M. Pastrana, C. Borrero, A. Rodríguez-Tello, M. Avilés, First report of root and crown rot caused by Fusarium oxysporum on Prunus cerasifera in Spain, Plant Dis. 108 (2024) 2218, https://doi.org/10.1094/PDIS-11-23-2411-PDN.
[21] A.F. Huamán, M. Arce, J. Huamán, V. Aguilar, S.M. Oliva, E. Hernández, Y. Fernández, T.J. Torres, J.R. Díaz-Valderrama, First report of basal rot of yellow dragon fruit (Selenicereus megalanthus) caused by Fusarium oxysporum in Peru, Plant Dis. (2024), https://doi.org/10.1094/pdis-05-24-1060-pdn.
[22] K.W. Brannan, I.A. Chaim, R.J. Marina, B.A. Yee, E.R. Kofman, D.A. Lorenz, P. Jagannatha, K.D. Dong, A.A. Madrigal, J.G. Underwood, G.W. Yeo, Robust single-cell discovery of RNA targets of RNA-binding proteins and ribosomes, Nat. Methods 18 (2021) 507–519, https://doi.org/10.1038/s41592-021-01128-0.
[23] R. Estrada, R. Cosme, T. Porras, A. Reynoso, C. Calderon, C.I. Arbizu, G.J. Arone, Changes in bulk and rhizosphere soil microbial diversity communities of native quinoa due to the monocropping in the Peruvian central andes, Microorganisms. 11 (2023), https://doi.org/10.3390/microorganisms11081926.
[24] M. Wang, C. Wang, Z. Yu, H. Wang, C. Wu, A. Masoudi, J. Liu, Fungal diversities and community assembly processes show different biogeographical patterns in forest and grassland soil ecosystems, Front. Microbiol. 14 (2023), https://doi.org/10.3389/fmicb.2023.1036905.
[25] D. Straub, N. Blackwell, A. Langarica-Fuentes, A. Peltzer, S. Nahnsen, S. Kleindienst, Interpretations of environmental microbial community studies are biased by the selected 16S rRNA (Gene) amplicon sequencing pipeline, Front. Microbiol. 11 (2020), https://doi.org/10.3389/fmicb.2020.550420.
[26] P.A. Ewels, A. Peltzer, S. Fillinger, H. Patel, J. Alneberg, A. Wilm, M.U. Garcia, P. Di Tommaso, S. Nahnsen, The nf-core framework for community-curated bioinformatics pipelines, Nat. Biotechnol. 38 (2020) 276–278, https://doi.org/10.1038/s41587-020-0439-x.
[27] B. D.R, S.G.R. Grüning, R. Dale, A. Sjamp, B.A. Chapman, J. Rowe, C.H. Tomkins-Tinch, R. Valieris, J. Kamp, Bioconda: sustainable and comprehensive software distribution for the life sciences, Nat. Methods 15 (2018) 475–476, https://doi.org/10.5281/zenodo.1068297.
[28] F. da Veiga Leprevost, Björn A. Grüning, R. Etournay, A. Sagner, S. Eaton, E. W. Myers, BioContainers: an open-source and community-driven framework for software standardization, Bioinformatics. 33 (2017) 1–7, https://doi.org/10.1093/bioinformatics/xxxxxx.
[29] P. Di Tommso, M. Chatzou, E.Wr Floden, F.M. Buffa, H.M. Marriott, J.M. Eales, M. P. Messenger, A.E. Anderson, C. Boot, C. Bunce, R.D. Goldin, J. Harris, R. F. Hinchliffe, H. Junaid, S. Kingston, C. Martin-Ruiz, C.P. Nelson, J. Peacock, P. T. Seed, B. Shinkins, K.J. Staples, J. Toombs, A.K.A. Wright, M. Dawn Teare, Nextflow enables reproducible computational workflows, Nature Biotechnology, Elife 4 (2017) 316–319, https://doi.org/10.7554/eLife.05519.
[30] S. Andrews, Babraham Bioinformatics - Fastqc A Quality Control Tool for High Throughput Sequence Data, 2010.
[31] P. Ewels, M. Magnusson, S. Lundin, M. Käller, MultiQC: Resumen de resultados de análisis para múltiples herramientas y muestras en un solo informe, Bioinformatics 32 (2016) 3047–3048, https://doi.org/10.1093/bioinformatics/btw354.
[32] B.J. Callahan, P.J. McMurdie, M.J. Rosen, A.W. Han, A.J.A. Johnson, S.P. Holmes, DADA2:Inferencia de muestras de alta resolución a partir de datos de amplicones de Illumina, Nat. Methods 13 (2016) 581–583, https://doi.org/10.1038/nmeth.3869.
[33] C. Quast, E. Pruesse, P. Yilmaz, J. Gerken, T. Schweer, P. Yarza, J. Peplies, F. O. Glöckner, The SILVA ribosomal RNA gene database project: improved data processing and web-based tools, Nucleic Acids Res. 41 (2013), https://doi.org/10.1093/nar/gks1219.
[34] E. Bolyen, J.R. Rideout, M.R. Dillon, N.A. Bokulich, C.C. Abnet, G.A. Al-Ghalith, H. Alexander, E.J. Alm, M. Arumugam, F. Asnicar, Y. Bai, J.E. Bisanz, K. Bittinger, A. Brejnrod, C.J. Brislawn, C.T. Brown, B.J. Callahan, A.M. Caraballo-Rodríguez, J. Chase, E.K. Cope, R. Da Silva, C. Diener, P.C. Dorrestein, G.M. Douglas, D. M. Durall, C. Duvallet, C.F. Edwardson, M. Ernst, M. Estaki, J. Fouquier, J. M. Gauglitz, S.M. Gibbons, D.L. Gibson, A. Gonzalez, K. Gorlick, J. Guo, B. Hillmann, S. Holmes, H. Holste, C. Huttenhower, G.A. Huttley, S. Janssen, A. K. Jarmusch, L. Jiang, B.D. Kaehler, K. Bin Kang, C.R. Keefe, P. Keim, S.T. Kelley, D. Knights, I. Koester, T. Kosciolek, J. Kreps, M.G.I. Langille, J. Lee, R. Ley, Y. X. Liu, E. Loftfield, C. Lozupone, M. Maher, C. Marotz, B.D. Martin, D. McDonald, L.J. McIver, A.V. Melnik, J.L. Metcalf, S.C. Morgan, J.T. Morton, A.T. Naimey, J. A. Navas-Molina, L.F. Nothias, S.B. Orchanian, T. Pearson, S.L. Peoples, D. Petras, M.L. Preuss, E. Pruesse, L.B. Rasmussen, A. Rivers, M.S. Robeson, P. Rosenthal, N. Segata, M. Shaffer, A. Shiffer, R. Sinha, S.J. Song, J.R. Spear, A.D. Swafford, L. R. Thompson, P.J. Torres, P. Trinh, A. Tripathi, P.J. Turnbaugh, S. Ul-Hasan, J.J. J. van der Hooft, F. Vargas, Y. Vázquez-Baeza, E. Vogtmann, M. von Hippel, W. Walters, Y. Wan, M. Wang, J. Warren, K.C. Weber, C.H.D. Williamson, A. D. Willis, Z.Z. Xu, J.R. Zaneveld, Y. Zhang, Q. Zhu, R. Knight, J.G. Caporaso, Reproducible, interactive, scalable and extensible microbiome data science using QIIME 2, Nat. Biotechnol. 37 (2019) 852–857, https://doi.org/10.1038/s41587-019-0209-9.
[35] G.M. Douglas, V.J. Maffei, J.R. Zaneveld, S.N. Yurgel, J.R. Brown, C.M. Taylor, C. Huttenhower, M.G.I. Langille, PICRUSt2 for prediction of metagenome functions, Nat. Biotechnol. 38 (2020) 685–688, https://doi.org/10.1038/s41587-020-0548-6.
[36] P.J. McMurdie, S. Holmes, Phyloseq: an R package for reproducible interactive analysis and graphics of microbiome census data, PLoS One 8 (2013), https://doi.org/10.1371/journal.pone.0061217.
[37] C. Liu, Y. Cui, X. Li, M. Yao, Microeco: an R package for data mining in microbial community ecology, FEMS Microbiol. Ecol. 97 (2021), https://doi.org/10.1093/femsec/fiaa255.
[38] S. Xu, L. Zhan, W. Tang, Q. Wang, Z. Dai, L. Zhou, T. Feng, M. Chen, T. Wu, E. Hu, G. Yu, MicrobiotaProcess: a comprehensive R package for deep mining microbiome, Innovation 4 (2023), https://doi.org/10.1016/j.xinn.2023.100388.
[39] E. Neuwirth, Rcolorbrewer: ColorBrewer Palettes (R Package Version 1.1-3), CRAN, 2022, https://doi.org/10.32614/CRAN.package.RColorBrewer. Contributed Packages.
[40] Z. Gu, ComplexHeatmap Citation (from within R, enter citation, "ComplexHeatmap")) (2016), https://doi.org/10.18129/B9.bioc.ComplexHeatmap.
[41] H. Wickham, ggplot2: Elegant Graphics for Data Analysis, Springer-Verlag, New York, 2016. https://exts.ggplot2.tidyverse.org/gallery/.
[42] A. Núñez, D.A. Moreno, The differential vertical distribution of the airborne biological particles reveals an atmospheric reservoir of microbial pathogens and aeroallergens, Microb. Ecol. 80 (2020) 322–333, https://doi.org/10.1007/s00248-020-01505-w.
[43] L. Cai, R. Jeewon, K.D. Hyde, Phylogenetic investigations of sordariaceae based on multiple gene sequences and morphology, Mycol. Res. 110 (2016) 137–150, https://doi.org/10.1016/j.mycres.2005.09.014.
[44] X. Zhou, J. Wang, F. Liu, J. Liang, P. Zhao, C.K.M. Tsui, L. Cai, Cross-kingdom synthetic microbiota supports tomato suppression of fusarium wilt disease, Nat. Commun. 13 (2022), https://doi.org/10.1038/s41467-022-35452-6.
[45] J.M. Chaparro, D.V. Badri, J.M. Vivanco, Rhizosphere microbiome assemblage is affected by plant development, ISME J. 8 (2014) 790–803, https://doi.org/10.1038/ismej.2013.196.
[46] R.S.C. De Souza, V.K. Okura, J.S.L. Armanhi, B. Jorrín, N. Lozano, M.J. Da Silva, M. González-Guerrero, L.M. De Araújo, N.C. Verza, H.C. Bagheri, J. Imperial, P. Arruda, Unlocking the bacterial and fungal communities assemblages of sugarcane microbiome, Sci. Rep. 6 (2016), https://doi.org/10.1038/srep28774.
[47] M. Chen, X. Li, Q. Yang, X. Chi, L. Pan, N. Chen, Z. Yang, T. Wang, M. Wang, S. Yu, Soil eukaryotic microorganism succession as affected by continuous cropping of peanut - pathogenic and beneficial fungi were selected, PLoS One. 7 (2012), https://doi.org/10.1371/journal.pone.0040659.
[48] S. Tafesse, C. Braam, B. van Mierlo, B. Lemaga, P.C. Struik, Association between soil acidity and bacterial wilt occurrence in potato production in Ethiopia, Agronomy 11 (2021), https://doi.org/10.3390/agronomy11081541.
[49] M. Naz, Z. Dai, S. Hussain, M. Tariq, S. Danish, I.U. Khan, S. Qi, D. Du, The soil pH and heavy metals revealed their impact on soil microbial community, J. Environ. Manag. 321 (2022), https://doi.org/10.1016/j.jenvman.2022.115770.